Journal of Alloys and Compounds 859 (2021) 157875

Contents lists available at ScienceDirect

Journal of Alloys and Compounds

journal homepage: http://www.elsevier.com/locate/jalcom

HfO_2/SiO_2 anti-reflection films for UV lasers via plasma-enhanced atomic layer deposition

Chaoyi Yin [a, b], Meiping Zhu [a, b, c, *], Tingting Zeng [a, b], Chen Song [a], Yingjie Chai [d], Yuchuan Shao [a, c], Rongjun Zhang [e], Jiaoling Zhao [a], Dawei Li [a], Jianda Shao [a, b, c, f, **]

[a] Laboratory of Thin Film Optics, Key Laboratory of Materials for High Power Laser, Shanghai Institute of Optics and Fine Mechanics, Chinese Academy of Sciences, Shanghai, 201800, China
[b] Center of Materials Science and Optoelectronics Engineering, University of Chinese Academy of Sciences, Beijing, 100049, China
[c] Hangzhou Institute for Advanced Study, University of Chinese Academy of Sciences, Hangzhou, 310024, China
[d] CREOL, The College of Optics and Photonics, University of Central Florida, Orlando, FL, 32816, USA
[e] Shanghai Engineering Research Center of Ultra-Precision Optical Manufacturing, Department of Optical Science and Engineering, Fudan University, Shanghai, 200433, China
[f] CAS Center for Excellence in Ultra-intense Laser Science, Shanghai, 201800, China

ARTICLE INFO

Article history:
Received 4 June 2020
Received in revised form
4 November 2020
Accepted 9 November 2020
Available online 19 November 2020

Keywords:
Plasma-enhanced atomic layer deposition
Low-temperature deposition
Anti-reflection films
High power lasers
Laser-induced damage threshold

ABSTRACT

The laser-induced damage threshold (LIDT) of HfO_2/SiO_2 anti-reflection (AR) films for ultraviolet (UV) lasers was improved via low-temperature plasma-enhanced atomic layer deposition (PEALD). Focused on the chemical composition, optical absorption, surface scattering, and laser-resistance, the impact of precursor exposure time on PEALD SiO_2 film properties and growth temperature on PEALD SiO_2 and HfO_2 film properties were investigated respectively. When irradiated by UV laser, PEALD SiO_2 film exhibits a higher LIDT than the PEALD HfO_2 film, which is consistent with their less impurity content and lower absorption. A bilayer structure HfO_2/SiO_2 AR film for 355 nm laser was designed and experimentally demonstrated via PEALD growth at a temperature of 150 °C. The prepared PEALD AR film shows a reflectance <0.2% at 355 nm as designed and better laser-damage resistance with a LIDT of 24.4 J/cm^2 (355 nm, 7.8 ns) than the conventional e-beam deposition method.

© 2020 Elsevier B.V. All rights reserved.

1. Introduction

High-power lasers have attracted growing interests in recent years for their applications in many areas, including clean energy [1], light-matter interaction [2], and communications [3]. Developing new thin-film optics that can endure in enormously high-power lasers is one of the main challenges [4].

Traditional high-resistance laser coatings were mostly prepared by electron-beam evaporation [5,6], ion-assisted deposition [7,8], ion-beam sputtering [9], and sol-gel method [10]. In recent years, atomic layer deposition (ALD) shows exceptionally precise thickness controllability [11], high uniformity [12], and unparalleled conformality [13]. Many works [14,15] have studied the influence of thermal ALD deposition parameters on the growth behavior, chemical composition, and electrical property. ALD also shows a high laser-induced damage threshold (LIDT) [16] and is a promising method for preparing thin films for high-power lasers applications [16,17]. Current attempts to prepare thin films for high power lasers via ALD focus on the use of TiO_2/Al_2O_3 or HfO_2/Al_2O_3 layers for near-infrared (NIR) anti-reflection (AR) films [17–20]. A high quality 1064 nm HfO_2/Al_2O_3 AR film prepared by ALD with an LIDT value of 30 J/cm^2 was reported by Zhang et al. [17]. There are relatively few reports on the use of ALD technology to prepare UV AR films. Most optical materials have large absorption in the UV region due to the limitation of optical bandgap width [21] and are sensitive to the absorption precursors such as defects [22] and impurities [23]. Also, nodules inside films have higher electric field intensification at the UV region [24], which is harmful to laser damage resistance of films [25]. Therefore, it is more difficult to obtain a high LIDT AR film in the UV region compared to the NIR

* Corresponding author. Laboratory of Thin Film Optics, Key Laboratory of Materials for High Power Laser, Shanghai Institute of Optics and Fine Mechanics, Chinese Academy of Sciences, Shanghai, 201800, China.
** Corresponding author. Laboratory of Thin Film Optics, Key Laboratory of Materials for High Power Laser, Shanghai Institute of Optics and Fine Mechanics, Chinese Academy of Sciences, Shanghai, 201800, China.
E-mail addresses: bree@siom.ac.cn (M. Zhu), jdshao@siom.ac.cn (J. Shao).

https://doi.org/10.1016/j.jallcom.2020.157875
0925-8388/© 2020 Elsevier B.V. All rights reserved.

region. Recently, a 355 nm AR film grown from HfO_2/Al_2O_3 layers with an LIDT of 4.5 J/cm^2 was reported by Hao Liu et al. [20]. However, the TiO_2/Al_2O_3 or HfO_2/Al_2O_3 design structures are not the best strategies for AR films for lasers in the UV to NIR wavelength region. According to a worldwide laser damage competition for UV AR films, HfO_2/SiO_2 films show the highest LIDT other than sol-gel SiO_2 films [26]. However, the sol-gel film suffers from chemical instability in ambient conditions [27,28]. SiO_2 is an ideal low refractive index material not only for coating quantum dots [29,30], but also for high-power laser applications from UV to NIR wavelength region because of its low loss and large optical bandgap properties [31,32]. Unfortunately, temperatures higher than 250 °C required for thermal ALD growth of SiO_2 [33,34] cause polycrystallization of HfO_2 film [35] and the shifting of sub-surface impurities to the surface of the substrate [36], which are not conducive to obtain AR film with high LIDT. Plasma-Enhanced ALD (PEALD), which provides similar growth characteristics as thermal ALD [37], has the advantage of low-temperature growth. It can increase the growth rate [12], better control the stoichiometry of materials [34,38], and allow larger freedom in processing conditions for tuning the properties of thin films [39]. We previously investigated the non-uniformity, surface roughness and simply compared the LIDT of PEALD SiO_2 and HfO_2 films [40], but further research is needed to study the performance of SiO_2 and HfO_2 films concerning their applications in laser systems. In this work, we aim to improve the LIDT of UV AR films via low-temperature PEALD growth of HfO_2/SiO_2 layers. In this method, O_2/Ar plasma is used to obtain high plasma density and achieve low-temperature growth and high growth rate [12]. The influence of precursor exposure time on growth characteristics of PEALD SiO_2 films was studied. The effects of growth temperature on the properties of both PEALD SiO_2 and HfO_2 films were investigated, especially the chemical composition, optical absorption, and laser damage resistant properties. A 355 nm AR film was then prepared for UV laser application via PEALD, the LIDT and damage mechanism were tested and analyzed.

2. Experimental

2.1. Preparation of PEALD SiO_2 and HfO_2 films

A commercial PEALD apparatus with an integrated remote plasma source (Picosun Advanced R200, Finland) was utilized. SiO_2 and HfO_2 films were deposited on a fused silica substrate or a BK7 glass substrate. The BK7 glass substrate was used to characterize the thicknesses of the film, while the fused silica substrate was used to investigate other properties of the film. To obtain a clear surface of the substrate, the fused silica substrate was first etched in a mixture solvent of ~1% HF and ~15% NH_4F for 8 min, then washed with deionized water in an ultrasonic bath for 5 min, and finally dried with an oven lamp. The BK7 glass substrate was cleaned using the last two steps of the cleaning procedure for a fused silica substrate.

The growth of SiO_2 and HfO_2 via PEALD was performed by alternately exposing the corresponding precursors - tris-dimethylamino silane ($SiH(N(CH_3)_2)_3$, 3DMAS) and tetrakis-ethylmethylamino hafnium ($Hf(N(CH_3)(CH_2CH_3))_4$, TEMAH), and O_2/Ar gas mixture plasma reactant. 3DMAS and TEMAH were injected into the chamber through the carrier gas N_2. The temperature of the 3DMAS source was maintained at room temperature, while the temperature of the TEMAH source was maintained at 120 °C. Three groups of films were prepared for comparative studies. Groups G1 and G2 are SiO_2 films, consisting of 750 SiO_2 growth cycles grown at different temperatures (in the range of 50–200 °C) and different exposure times (in the range of 0.1–0.7 s), respectively. The sequence of pulses for one cycle deposition of the SiO_2 film was as follows: 3DMAS feeding (0.1 s or 0.1–0.7 s), N_2 purging (19 s), O_2 feeding (11 s) with RF plasma power of 2500W, and Ar purging (8 s). The exposure time of the 3DMAS precursor of the SiO_2 films in group G1 was 0.1 s, and the deposition temperature of the SiO_2 films in group G2 was 150 °C. Group G3 is HfO_2 films, consisting of 500 cycles grown at different temperatures (in the range of 50–200 °C). The sequence of pulses for one cycle deposition of the HfO_2 film was as follows: TEMAH feeding (1.6 s), N_2 purging (19 s), O_2 feeding (11 s) with 2500W RF plasma power, and Ar purging (10 s).

2.2. Preparation of PEALD and E-beam 355 nm AR films

355 nm AR films were prepared using PEALD and e-beam deposition for comparative studies. The AR film was grown on fused silica substrates that were cleaned using the cleaning procedure of the three steps described above. The recipe of the PEALD AR film is given in terms of PEALD cycle sequences and shown as follows: 230 cycles $\times$ HfO_2 + 698 cycles $\times$ SiO_2, thereby obtaining a HfO_2 layer with a designed thickness of 20.1 nm and a SiO_2 layer with a designed thickness of 76.1 nm. The exposure time of 3DMAS precursor of SiO_2 film was 0.4 s, the growth temperature was 150 °C. Other growth parameters were consistent with the growth parameters of SiO_2 and HfO_2 films. Table 1 shows further deposition details.

The coating structure and layer thickness of the e-beam deposited AR film are the same as those of PEALD AR film. The coating chamber was heated to 150 °C before deposition. HfO_2 and SiO_2 layers were evaporated from metal Hf and SiO_2 materials at the deposition rates of 0.04 nm/s and 0.6 nm/s, respectively. The oxygen pressure of HfO_2 and SiO_2 were 2.8×10^{-2} Pa and 5×10^{-3} Pa, respectively.

2.3. Thin-film characterizations

The thickness and refractive index of the SiO_2 and HfO_2 films were determined by using a spectroscopic ellipsometer (Horiba Uvisel 2) and the Tauc-Lorentz model of the DeltaPsi2 software. The scattering of SiO_2 and HfO_2 films at 632.8 nm was measured by a

Table 1
Deposition parameters for PEALD AR film.

		HfO_2	SiO_2
Exposure time (s)	Precursor	1.6	0.4
	Plasma O_2	11	11
Purge time (s)	Precursor	19	19
	Plasma O_2	10	8
Boosting time (s)		1.7	/
Picoflow time (s)		/	11
Growth temperature (°C)		150	150
Number of cycles		230	698

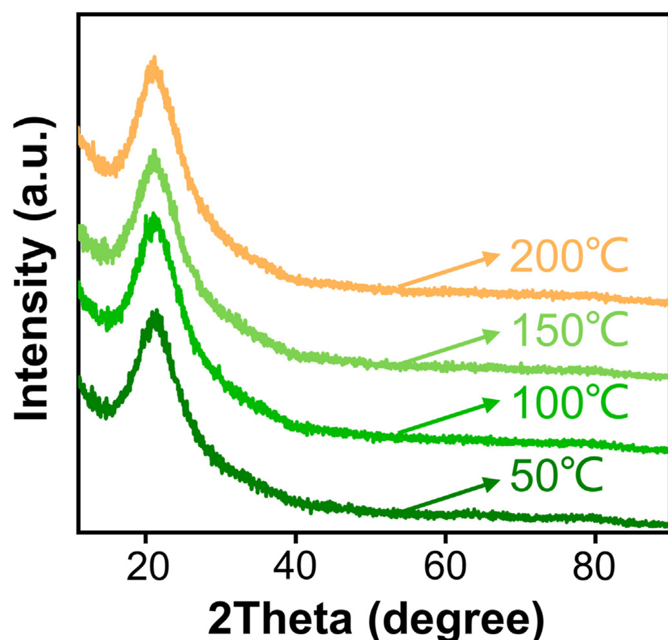

Fig. 1. XRD spectra of PEALD SiO_2 films grown at different temperatures.

home-made system based on a total integrated scattering method [41]. The structural information was measured by X-ray diffraction (XRD, PanAlytical Empyrean). The film absorption at 355 nm was measured by a home-made system based on the surface thermal lensing technique [42]. The 355 nm laser power irradiated on the film was in the range of 99.5–291.7 W/mm^2. The absorption value of each SiO_2 film was recorded for 600 s, and the average value was taken as the absorption. For HfO_2 and 355 nm AR films, the absorption value decreases with the laser irradiation time before reaching a stable value. The absorption value of each HfO_2 film and 355 nm AR film was recorded for 2000 s, and the average value at the stable stage was taken as the absorption. The chemical composition of the SiO_2 and HfO_2 films was analyzed by an X-ray photoelectron spectroscopy (XPS, Thermo Scientific) equipped with a monochromatic Al Kα (1486.6 eV) X-ray source. To remove the surface layer which adsorbs water and oxygen in the air, the coating was etched for 80 s with 1 keV Ar^+ ions before the XPS scan. The binding energy of the C 1s line is taken as 284.8 eV for calibrating the obtained spectra. The reflectance spectrum was measured by a UV–visible spectrometer (PerkinElmer Lambda 1050) at normal incidence. The 1-on-1 LIDT was measured according to ISO 21254 using a Gaussian-shape 3ω Nd: YAG laser (355 nm, 7.8 ns). The LIDT test was performed under normal incidence, and the effective spot area on the sample surface was 0.28 mm^2. The maximum fluence with zero probability of laser damage was determined as LIDT. The surface and cross-section morphologies of the laser-induced damaged site were obtained by a focused ion-beam scanning electron microscope (FIB-SEM, Carl Zeiss AURIGA CrossBeam). The chemical composition of the laser-induced damaged site was analyzed by an energy dispersive spectroscopy (EDS, Oxford X-Max, 50 mm^2), operated at an accelerating voltage of 15 kV. Before FIB-SEM and EDS characterization, a 20 nm-thick Cr film was deposited on the sample surface by ion beam sputtering (Quorum Q150T ES).

3. Results and discussions

3.1. Properties of the SiO_2 films in group G1

The ellipsometrically determined thicknesses of SiO_2 films grown at 50, 100, 150, and 200 °C are 88.1, 83.9, 83.2, and 73.7 nm, respectively. Fig. 1 shows XRD spectra of the SiO_2 films, and no

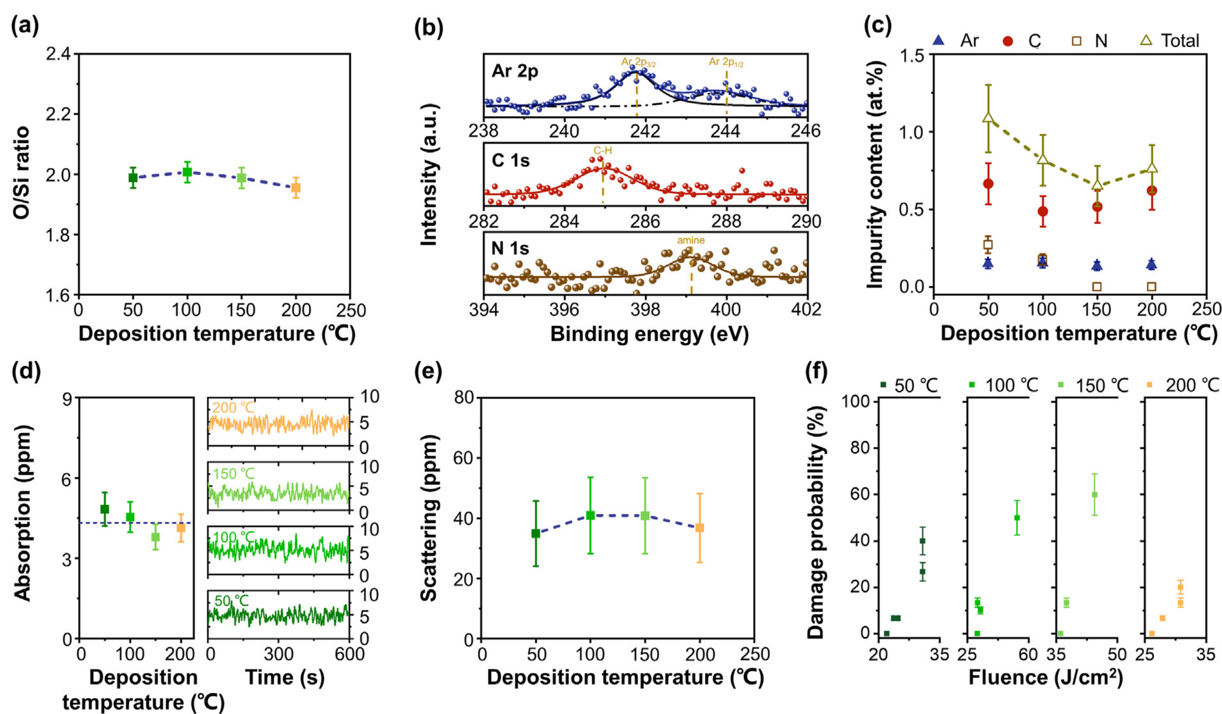

Fig. 2. (a) O/Si ratio of PEALD SiO_2 films in Group G1. (b) A typical XPS spectrum of Ar 2p, C 1s, and N 1s in a PEALD SiO_2 film grown at 100 °C. (c) Individual and total impurity contents of Ar, C, and N elements, (d) absorption measured at 355 nm, (e) scattering measured at 632.8 nm, and (f) laser-induced damage probability for PEALD SiO_2 films in Group G1. The dash-dot line in (d) shows the average absorption of PEALD SiO_2 films grown at different temperatures.

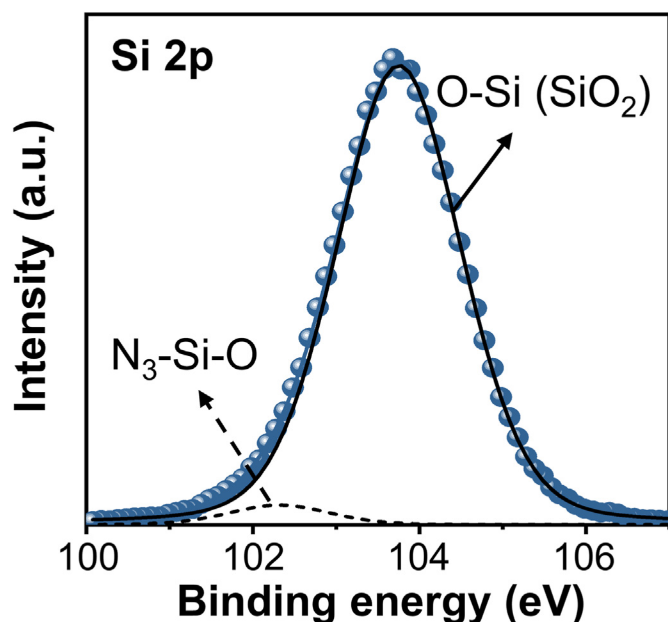

Fig. 3. A typical Si 2p spectrum of a PEALD SiO_2 film deposited at a temperature of 100 °C.

peak is observed except for a broad peak corresponding to the fused silica substrate, which indicates that the SiO_2 film is amorphous. XPS was used to examine the chemical composition and bonding structure of the SiO_2 films. The O/Si ratio determined by XPS is shown in Fig. 2a, and the O/Si ratio of the SiO_2 film deposited at 50, 100, and 150 °C is close to the stoichiometric ratio of 2. As the deposition temperature further increases, the O/Si ratio of the PEALD SiO_2 film decreases. Ar and C elements are observed in all SiO_2 films, but N element is only observed in SiO_2 films deposited at temperatures of 50 and 100 °C. Fig. 2b shows typical XPS spectra of Ar, C, and N in a SiO_2 film grown at a temperature of 100 °C. Two noticeable peaks, at 241.8 eV (Ar $2p_{3/2}$) and 243.9 eV (Ar $2p_{1/2}$), are observed in the Ar 2p spectrum, which is in agreement with previously reported binding energies [43]. The peak at 284.9 eV in the C 1s spectrum is related to the C—H bond [44]. The peak at 399.1 eV in the N 1s spectrum is associated with the undoped amine unit [45], which comes from the 3DMAS precursor. A typical Si 2p spectrum of a SiO_2 film deposited at a temperature of 100 °C is shown in Fig. 3 and can be fitted with two Gaussian peaks. The binding energy of Si 2p peak located at 103.7 eV corresponds to the Si—O bond of SiO_2 [46]. The lower binding energy of Si 2p peak located at 102.3 eV corresponds to the N_3—*Si*—O bond [47], indicating the presence of residual 3DMAS in the SiO_2 film. The individual and total contents of the Ar, C, and N elements in the SiO_2 films are shown in Fig. 2c. As the deposition temperature increases, the total impurity content decreases first and then increases. The SiO_2 film deposited at a temperature of 150 °C shows the lowest impurity content. The absorption and scattering of SiO_2 films are shown in Fig. 2d and e, respectively. All SiO_2 films show pretty low absorption, which fluctuates with the measurement time. The scattering of SiO_2 film is relatively low and corresponds to the low roughness of SiO_2 film [40]. The laser-induced damage probability of the SiO_2 films is compared in Fig. 2f. The SiO_2 film deposited at a temperature of 150 °C exhibits the highest LIDT, which is consistent with the lowest impurity content observed.

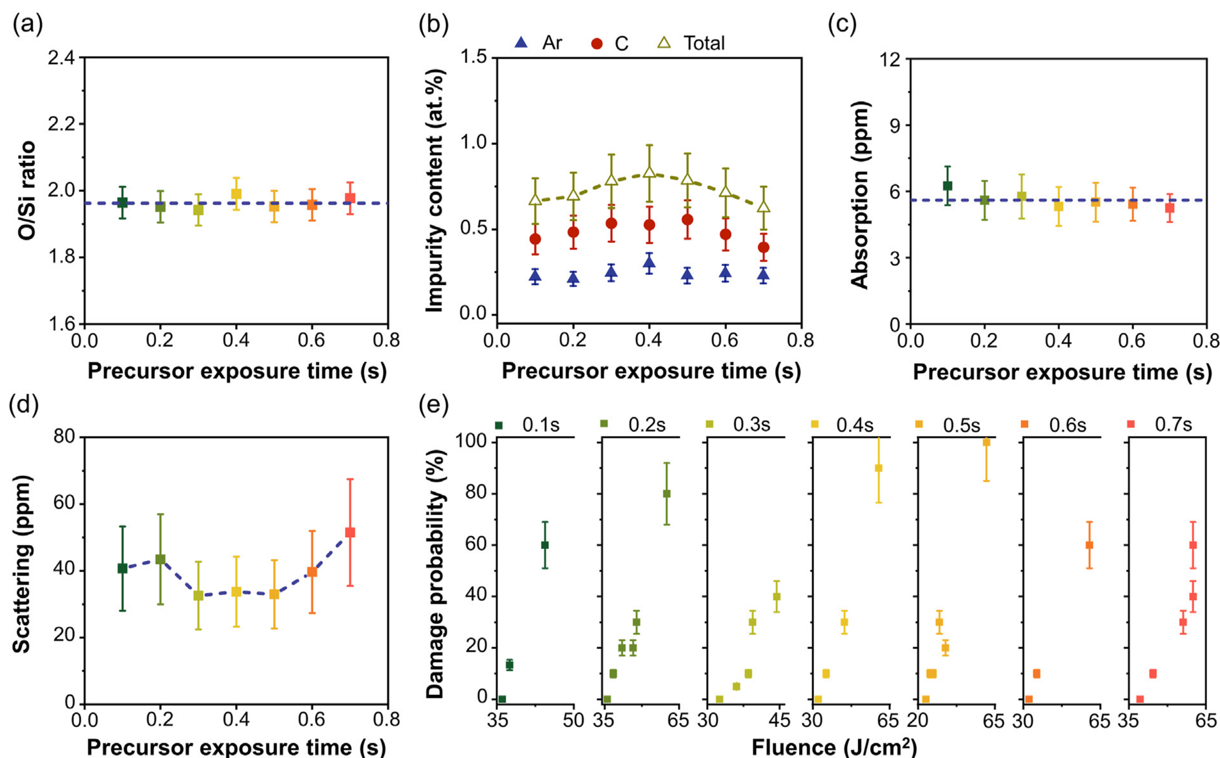

Fig. 4. (a) O/Si ratio, (b) individual and total impurity contents of Ar and C, (c) absorption measured at 355 nm, (d) scattering measured at 632.8 nm, and (e) laser-induced damage probability for PEALD SiO_2 films in Group G2. The dash-dot lines in (a) and (c) show the average O/Si ratio and absorption of PEALD SiO_2 films grown at different precursor exposure times.

3.2. Properties of the SiO_2 films in group G2

The ellipsometrically determined thicknesses of SiO_2 films grown at 0.1, 0.2, 0.3, 0.4, 0.5, 0.6 and 0.7 s are 69.0, 73.9, 76.5, 77.1, 77.8, 77.6 and 75.1 nm, respectively. The XPS determined O/Si ratio of the SiO_2 films is close to the stoichiometric ratio of 2, as shown in Fig. 4a. Ar and C elements are observed in all SiO_2 films prepared with different precursor exposure times, while the N element is not observed. The individual and total impurity contents of Ar and C of the SiO_2 films are shown in Fig. 4b. When the precursor exposure time is longer than 0.4 s, the impurity content decreases slightly with the increase of the precursor exposure time. The absorption and absorption curve versus the measurement time of the SiO_2 films are shown in Figs. 4c and 5. The absorption of SiO_2 films is relatively low and fluctuates around 5.6 ppm with increasing precursor exposure time. Compared with SiO_2 films deposited with other precursor exposure times, the SiO_2 film deposited with the precursor exposure time in the range of 0.3–0.5 s shows lower scattering, as shown in Fig. 4d. Light scattering normally increases with surface roughness [48]. The lower scattering of the SiO_2 film deposited with the precursor exposure time in the range of 0.3–0.5 s corresponds to the lower surface roughness in our previous work [40]. Fig. 4e shows the laser-induced damage probability versus the input fluence of the films deposited at different precursor exposure times, indicating that the PEALD SiO_2 films grown at precursor exposure times in the range of 0.4–0.6 s exhibit relatively lower LIDT, which is due to the higher impurity content and therefore more absorption defects [23]. Although the LIDT of a PEALD SiO_2 film grown with a precursor exposure time of 0.4 s is slightly lower than the highest observed LIDT, the precursor exposure time of 0.4 s was chosen as a parameter for the preparation of the SiO_2 layer in the UV AR film because it facilitates the thickness uniformity [40].

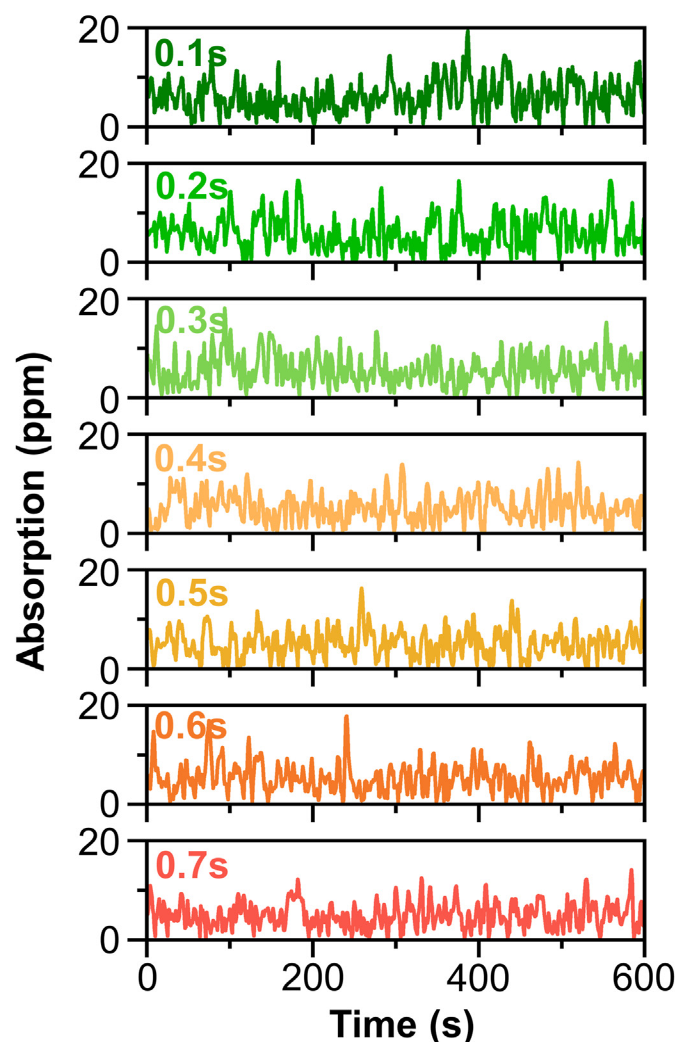

Fig. 5. The absorption curves at 355 nm versus measurement time of PEALD SiO_2 films grown at different precursor exposure times.

3.3. Properties of the HfO_2 films of group G3

The ellipsometrically determined thicknesses of HfO_2 films grown at 50, 100, 150, and 200 °C are 72.4 nm, 57.3 nm, 51.5 nm, and 47.7 nm, respectively. The XRD spectra indicate that the HfO_2 films tend to crystallize with increasing temperature, as shown in Fig. 6a. Fig. 6b shows that the O/Hf ratio of the HfO_2 film grown at a temperature of 150 °C is the highest, and the scattering of the HfO_2 films grown at 150 and 200 °C is relatively lower than other temperatures. The chemical composition characterized by XPS indicates that Ar, C, and N elements are present in all HfO_2 films. Fig. 6c shows a typical XPS spectrum of Ar, C, and N elements in a HfO_2 film deposited at 200 °C. In addition to the two peaks at 241.9 eV (Ar $2p_{3/2}$) and 243.9 eV (Ar $2p_{1/2}$), which are inconsistent with that observed in SiO_2 film, another peak at 238.8 eV is observed in the Ar 2p spectrum corresponding to N *KLL* Auger [42]. Two noticeable peaks—at 285.0 eV and 289.0 eV—are observed in the C 1s spectrum, corresponding to the C–H bond and O–C=O bond, respectively [44]. In the core level spectrum of N 1s, in addition to the peak at 399.1 eV associated with the undoped amine unit, a peak at 395.8 eV associated with the Hf–N bond from Hf precursor is observed [45,49]. A typical Hf 4f spectrum of a HfO_2 film deposited at a temperature of 200 °C is shown in Fig. 7a and can be fitted into two groups of Hf 4f peaks. Each Hf 4f peak shows a sharp doublet according to spin-orbit splitting into the Hf $4f_{5/2}$ and Hf $4f_{7/2}$ with the splitting binding energy of ~1.7 eV in good agreement with the theoretical value. The binding energy of the Hf $4f_{7/2}$ peak located at 16.8 eV represents the Hf–O bond of HfO_2 [50]. The lower binding energy of the Hf $4f_{7/2}$ peak located at 15.9 eV represents the Hf–N bond [51], which indicates the presence of residual TEMAH precursor in HfO_2 film. A typical O 1s spectrum of a HfO_2 film deposited at a temperature of 200 °C is shown in Fig. 7b and can be fitted into two Gaussian peaks, centered at 530.3 eV (O–Hf) and 532.1 eV (Hf–O–C) [44], respectively. The presence of the O 1s peak at 532.1 eV and C 1s peak at 289 eV may indicate that precursor residues in the HfO_2 film were further oxidized by plasma oxygen. The individual and total contents of Ar, C, and N in the HfO_2 films are shown in Fig. 6d. Overall, the impurity contents in HfO_2 films are quite high, and the total impurity content in some HfO_2 films is even higher than 10%. The total impurity content of the HfO_2 film first increases with the increase of the deposition temperature, which may be due to the enhancement of chemisorption caused by the increase of chemical activity of the precursor [52]. When the deposition temperature is higher than 150 °C, the precursor tends to decompose due to the limited thermal stability [53], and the impurity content accordingly decreases with the deposition temperature. All HfO_2 films exhibit a large absorption as shown in Fig. 6e. The absorption of HfO_2 films decreases with measurement time and becomes stable after approximately 1500 s. This absorption annealing effect of HfO_2 films is possibly due to the interaction of 355-nm laser radiation with surface defects [54]. When the deposition temperature is lower than 150 °C, the film absorption is mainly caused by impurities, and increases with increasing deposition temperature. Although the HfO_2 film grown

at 200 °C shows a lower impurity content than the HfO_2 film grown at 150 °C, it shows a larger absorption, which may be due to lower reactive-site (such as hydroxyl) density [55] and therefore more oxygen vacancies caused by incomplete oxidation at high temperature [56]. The laser damage probability of the HfO_2 films is compared in Fig. 6f. The LIDT of HfO_2 films decreases with increasing temperature, which corresponds to the higher impurity content and lower O/Hf ratio at high temperatures.

3.4. 355 nm AR films for high power lasers

A HfO_2/SiO_2 double-layer AR film was designed to achieve a reflectance <0.2% at 355 nm. The growth temperature of the PEALD AR film was selected to be 150 °C for two reasons. First, the SiO_2 layer is on top of the HfO_2 layer and will be directly exposed to laser radiation. Secondly, the thickness of HfO_2 is much thinner than that of SiO_2. The temperature that is beneficial to obtain a SiO_2 film with a higher LIDT is more favorable for obtaining an AR film with a higher LIDT.

As shown in Fig. 8a, the measured reflectance of both PEALD and e-beam AR films is lower than 0.2% as designed. The absorption curves versus measurement time of the PEALD and e-beam deposited AR films are shown in Fig. 8b. The absorption of the PEALD AR film is lower than the e-beam deposited AR film. The decreasing absorption of both PEALD and e-beam AR films versus measurement time is mostly due to the annealing effect of the underlying HfO_2 layer. The laser damage probability of the PEALD and e-beam deposited AR films as a function of the input fluence is compared in Fig. 8c. The LIDT of the PEALD AR film (24.4 J/cm^2) is higher than that of the e-beam AR film (20.6 J/cm^2), which

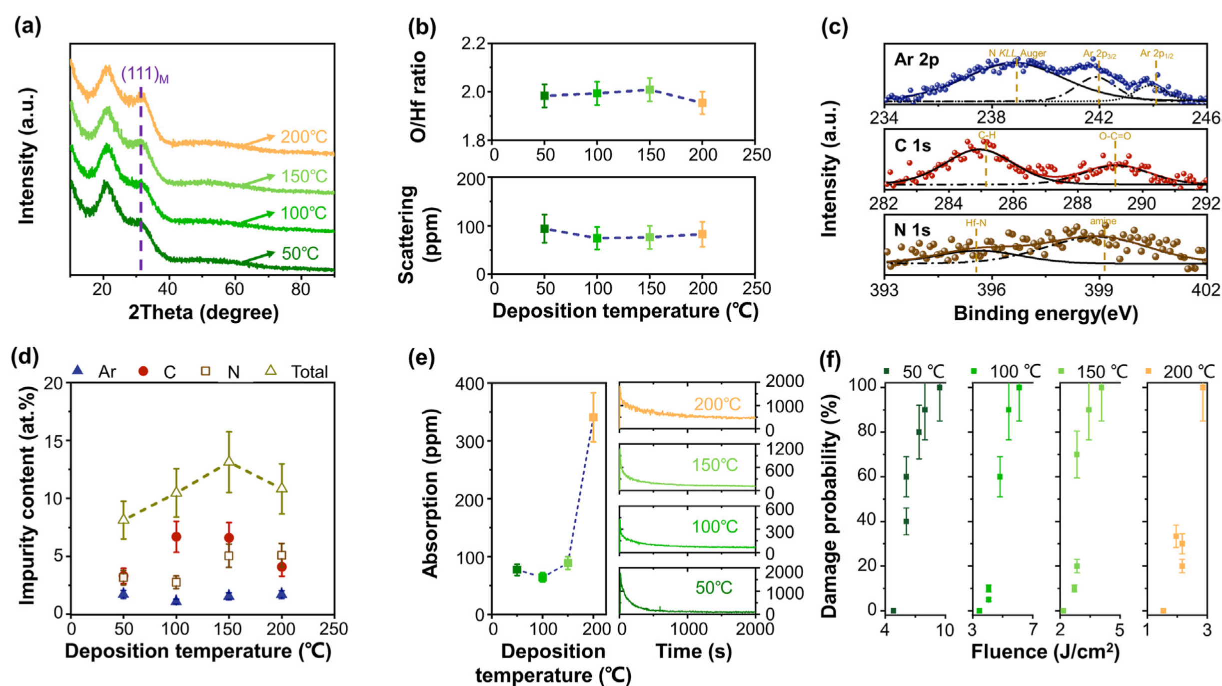

Fig. 6. (a) XRD spectra, (b) O/Hf ratio, and scattering measured at 632.8 nm of the PEALD HfO_2 films in Group G3. (c) A typical XPS spectrum of Ar 2p, C 1s, and N 1s in a PEALD HfO_2 film grown at 200 °C. (d) Individual and total impurity contents of Ar, C, and N elements, (e) absorption measured at 355 nm, (f) laser-induced damage probability for PEALD HfO_2 films in Group G3.

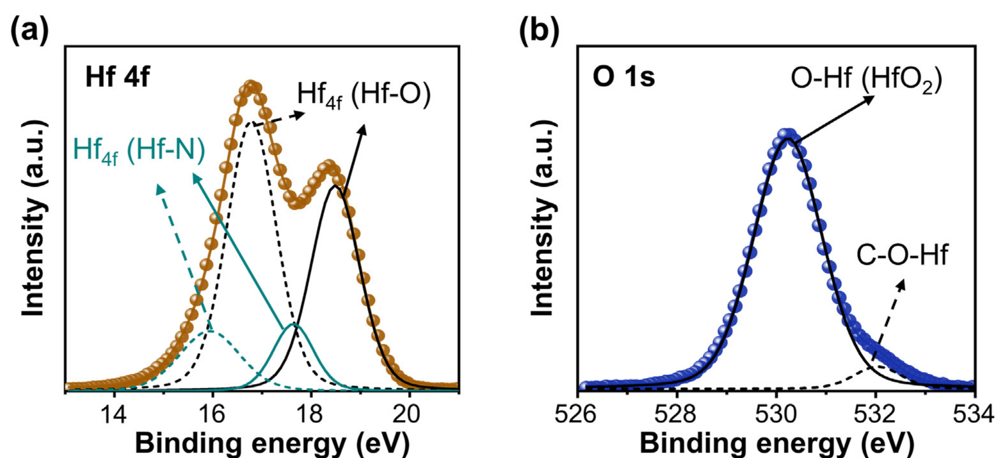

Fig. 7. The typical (a) Hf 4f spectrum and (b) O 1s spectrum of a PEALD HfO_2 film deposited at a temperature of 200 °C.

corresponds to the lower absorption of the PEALD AR film. The laser-induced damage probability of the fused-silica substrate with the same cleaning procedure as AR film is also shown in Fig. 8c for comparison.

The laser-induced damage morphology of PEALD AR film was characterized by FIB-SEM to investigate the laser-induced damage mechanism of PEALD AR film. As shown in Fig. 8, the typical damage morphology of a PEALD AR film is different from the observed pit damage morphology in a PEALD SiO_2 film and the ablation damage morphology in a PEALD HfO_2 film [40]. As shown in Fig. 8d, the damage morphology induced by a near-LIDT laser fluence indicates the formation of a blister and the bucking is initially located at the interface of HfO_2 and SiO_2 layers, which may be due to the high interface defect density [6,40], poor interfacial adhesion [57], and the stress mismatch of HfO_2 and SiO_2 layers [58,59]. At a higher laser fluence, the top SiO_2 layer has been stripped away (Fig. 8e), and no Hf element was observed in the EDS scan of the center area of the damaged site (Fig. 9), suggesting that the underlying HfO_2 layer is completely ablated at a higher laser fluence. As the laser fluence further increases, laser damage will penetrate the fused silica substrate, and a shell-like pit similar to the damage morphology of fused silica is observed in the center of the damaged area (Fig. 8f).

The damage morphology suggests that the initial damage of the PEALD AR film is closely related to the HfO_2 layer. Measures that can reduce impurity content and film absorption of the HfO_2 layer, including post-annealing [60] and incorporation of Al_2O_3 [61], may further improve the LIDT performance.

4. Conclusion

PEALD SiO_2 and HfO_2 films were prepared, and the properties related to UV laser applications were studied. Through a comprehensive analysis of the chemical composition, absorption, scattering and laser-induced damage property of PEALD SiO_2 and HfO_2 films, we confirmed that PEALD SiO_2 films have lower impurity content and absorption, and therefore show higher LIDT than PEALD HfO_2 films. This makes PEALD SiO_2 films suitable for UV laser applications. A bilayer structure HfO_2-SiO_2 AR film for 355 nm lasers was designed and fabricated via PEALD and e-beam deposition. The reflectance and LIDT of the PEALD AR films were investigated and compared with e-beam AR films. The reflectance of both AR films is lower than 0.2% as designed. The LIDT of the PEALD AR film (24.4 J/cm^2) is higher than that of the e-beam AR film (20.6 J/cm^2). The laser-induced damage morphology suggests that the laser-induced damage of PEALD AR film is closely related to the HfO_2

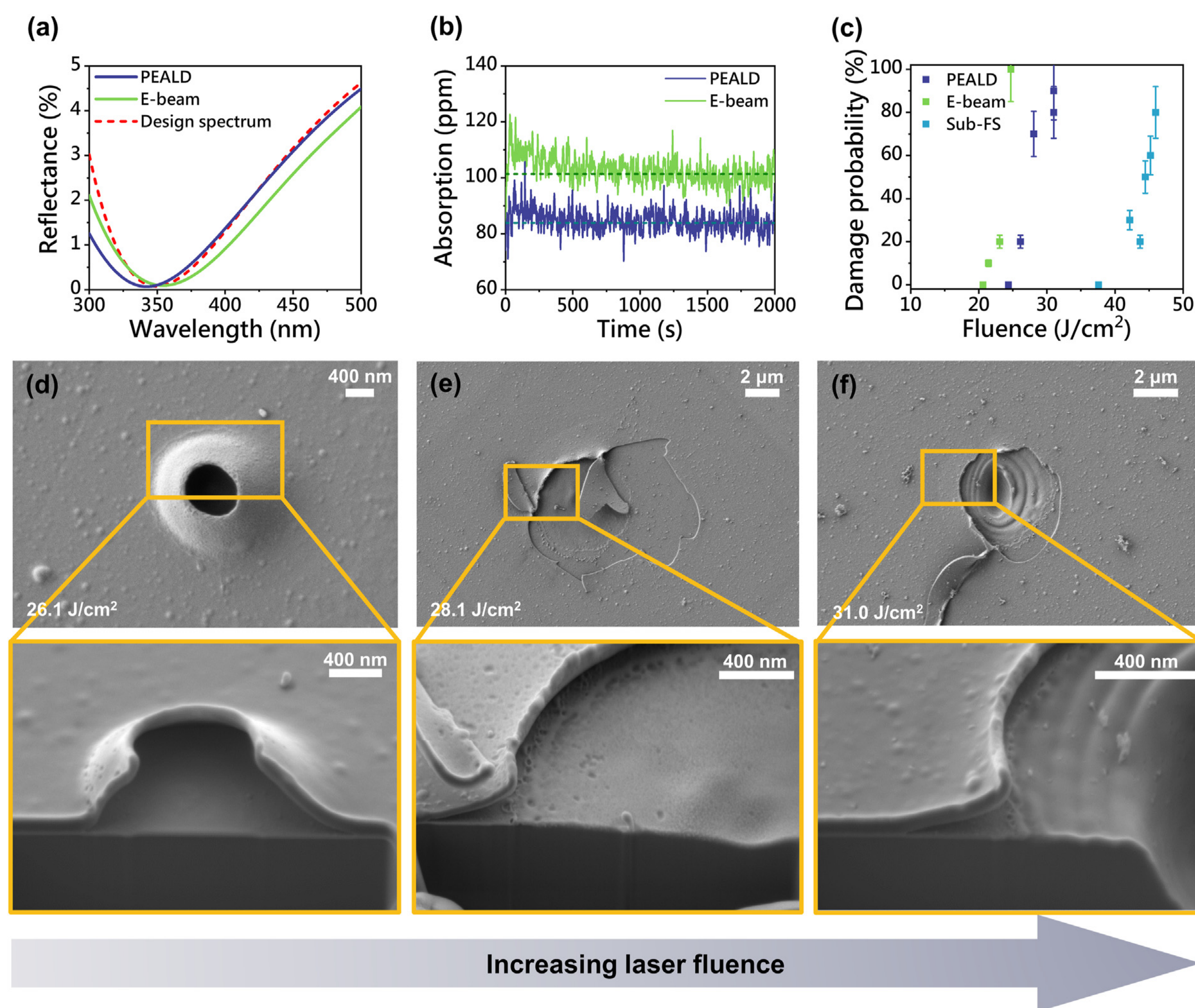

Fig. 8. (a) Measured reflectance spectra, (b) absorption curves versus measurement time, and (c) laser-induced damage probability of the PEALD and e-beam AR films and fused-silica substrate. The dash-dot line in (b) shows the average absorption between 1900 s and 2000 s of the measurement time. (d–f) Damaged sites imaged by SEM and the depth profiles of the marked regions measured by FIB.

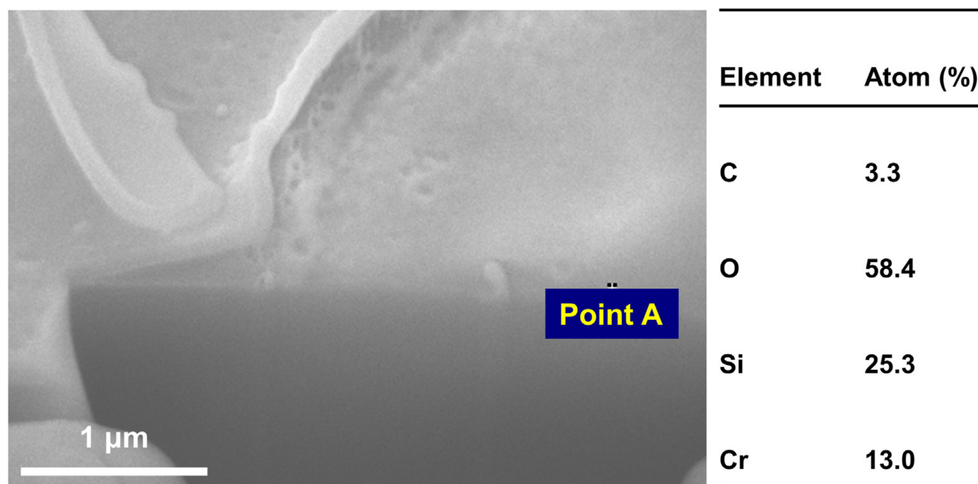

Fig. 9. EDS characterized element content of point 'A' in the center area of the damaged site of a PEALD AR film irradiated by a laser fluence of 28.1 J/cm^2.

layer. Further improvement of LIDT may be achieved by Al_2O_3 incorporation and post-annealing. PEALD-grown HfO_2-SiO_2 film is expected to be promising in AR films for laser applications.

CRediT authorship contribution statement

Chaoyi Yin: Conceptualization, Methodology, Formal analysis, Data curation, Writing - original draft, Visualization. **Meiping Zhu:** Validation, Writing - review & editing, Supervision, Project administration, Funding acquisition. **Tingting Zeng:** Validation, Formal analysis, Data curation, Writing - review & editing. **Chen Song:** Investigation, Resources. **Yingjie Chai:** Software, Formal analysis, Writing - review & editing. **Yuchuan Shao:** Validation, Project administration. **Rongjun Zhang:** Validation, Supervision. **Jiaoling Zhao:** Resources, Writing - review & editing. **Dawei Li:** Investigation, Supervision. **Jianda Shao:** Project administration, Funding acquisition.

Declaration of competing interest

The authors declare that they have no known competing financial interests or personal relationships that could have appeared to influence the work reported in this paper.

Acknowledgements

The authors express their appreciation to Yun Cui and Yuan'an Zhao for the FIB and LIDT measurements, respectively. This work is supported by the National Natural Science Foundation of China [Grant No.61975215; Grant No.U1831211]; the National Special Support Program for Young Top-notch Talent; the Youth Innovation Promotion Association of the Chinese Academy of Sciences; the Shanghai Young Top-notch Talent Program; and the Strategic Priority Research Program of Chinese Academy of Sciences [Grant No. XDA25020000; Grant No.XDB16030400].

References

[1] C. MacIlwaln, Inadequate optics "threat to US laser facility,", Nature. 403 (2000) 120, https://doi.org/10.1038/35003273.
[2] Extreme light, Nat. Mater. 15 (2015) 1, https://doi.org/10.1038/nmat4533.
[3] C. Jauregui, J. Limpert, A. Tünnermann, High-power fibre lasers, Nat. Photon. 7 (2013) 861–867, https://doi.org/10.1038/nphoton.2013.273.
[4] P. Norvig, D.A. Relman, D.B. Goldstein, D.M. Kammen, D.R. Weinberger, L.C. Aiello, G. Church, J.L. Hennessy, J. Sachs, A. Burrows, G.P. Pisano, J.R. Goldstein, P. Anastas, R. Klausner, D. Baltimore, D.R. Montgomery, T.M. Baer, N.P. Bigelow, R.D. Holt, J.K. Nicholson, 2020 visions, Nature 463 (2010) 26–32, https://doi.org/10.1038/463026a.
[5] E.S. Field, B. Galloway, D. Kletecka, P. Rambo, I. Smith, Dual-wavelength laser-induced damage threshold of a HfO_2/SiO_2 dichroic coating developed for high transmission at 527 nm and high reflection at 1054 nm, Proc. SPIE 11173 (2019) 14, https://doi.org/10.1117/12.2536417.
[6] H. Xing, M. Zhu, Y. Chai, K. Yi, J. Sun, Y. Cui, J. Shao, Improving laser damage resistance of 355 nm high-reflective coatings by co-evaporated interfaces, Opt. Lett. 41 (2016) 1253–1256, https://doi.org/10.1364/ol.41.001253.
[7] X. Cheng, S. Dong, S. Zhi, S. Paschel, I. Balasa, D. Ristau, Z. Wang, Waterproof coatings for high-power laser cavities, Light Sci. Appl. 8 (2019) 1–6, https://doi.org/10.1038/s41377-018-0118-6.
[8] A.Q. Wang, J. Wang, M.J. D'Lallo, J.E. Platten, J.C. Crifasi, B.P. Roy, HfO_2/SiO_2 multilayer enhanced aluminum alloy-based dual-wavelength high reflective optics, Thin Solid Films 592 (2015) 232–236, https://doi.org/10.1016/j.tsf.2015.04.032.
[9] S. Malobabic, M. Jupé, D. Ristau, Spatial separation effects in a guiding procedure in a modified ion-beam-sputtering process, Light Sci. Appl. 5 (2016), https://doi.org/10.1038/lsa.2016.44 e16044–e16044.
[10] X. Li, M. Gross, K. Green, B. Oreb, J. Shen, Ultraviolet laser-induced damage on fused silica substrate and its sol-gel coating, Opt. Lett. 37 (2012) 2364–2366, https://doi.org/10.1364/ol.37.002364.
[11] C. Mahata, Y.C. Byun, C.H. An, S. Choi, Y. An, H. Kim, Comparative study of atomic-layer-deposited stacked (HfO_2/Al_2O_3) and nanolaminated ($HfAlO_x$) dielectrics on $In_{0.53}Ga_{0.47}As$, ACS Appl. Mater. Interfaces 5 (2013) 4195–4201, https://doi.org/10.1021/am400368x.
[12] H. Jung, I.K. Oh, C.M. Yoon, B.E. Park, S. Lee, O. Kwon, W.J. Lee, S.H. Kwon, W.H. Kim, H. Kim, Effects of Ar addition to O_2 plasma on plasma-enhanced atomic layer deposition of oxide thin films, ACS Appl. Mater. Interfaces 10 (2018) 40286–40293, https://doi.org/10.1021/acsami.8b14244.
[13] T. Faraz, H.C.M. Knoops, M.A. Verheijen, C.A.A. Van Helvoirt, S. Karwal, A. Sharma, V. Beladiya, A. Szeghalmi, D.M. Hausmann, J. Henri, M. Creatore, W.M.M. Kessels, Tuning material properties of oxides and nitrides by substrate biasing during plasma-enhanced atomic layer deposition on planar and 3D substrate topographies, ACS Appl. Mater. Interfaces 10 (2018) 13158–13180, https://doi.org/10.1021/acsami.8b00183.
[14] E.P. Gusev, C. Cabral, M. Copel, C. D'Emic, M. Gribelyuk, Ultrathin HfO_2 films grown on silicon by atomic layer deposition for advanced gate dielectrics applications, Microelectron. Eng. 69 (2003) 145–151, https://doi.org/10.1016/S0167-9317(03)00291-0.
[15] L. Bartholomew, C. Barelli, J. Owyang, R. DiCarlo, D. Shenai, C. Marsman, Y. Senzaki, Comparison of ALD of HfO_2, SiO_2, and $HfSiO_x$ thin films using various metal/silicon alkylamide precursors and O_3, ECS Trans 3 (2019) 37–49, https://doi.org/10.1149/1.2721472.
[16] H. Liu, L. Jensen, P. Ma, D. Ristau, Stress compensated anti-reflection coating for high power laser deposited with IBS SiO_2 and ALD Al_2O_3, Appl. Surf. Sci. 476 (2019) 521–527, https://doi.org/10.1016/j.apsusc.2019.01.125.
[17] Q. Zhang, F. Pan, J. Luo, Q. Wu, Z. Wang, Y. Wei, Optical and laser damage properties of HfO_2/Al_2O_3 thin films deposited by atomic layer deposition, J. Alloys Compd. 659 (2016) 288–294, https://doi.org/10.1016/j.jallcom.2015.11.048.
[18] Y. Wei, H. Liu, O. Sheng, Z. Liu, S. Chen, L. Yang, Laser damage properties of TiO_2/Al_2O_3 thin films grown by atomic layer deposition, Appl. Optic. 50 (2011) 4720–4727, https://doi.org/10.1364/AO.50.004720.
[19] Z. Liu, S. Chen, P. Ma, Y. Wei, Y. Zheng, F. Pan, H. Liu, G. Tang, Characterization of 1064 nm nanosecond laser-induced damage on antireflection coatings

grown by atomic layer deposition, Optic Express 20 (2012) 854–863, https://doi.org/10.1364/oe.20.000854.
[20] H. Liu, L. Jensen, D. Ristau, ALD anti-reflection coatings at 1ω, 2ω, 3ω, and 4ω for high-power ns-laser application, Adv. Opt. Technol. 7 (2018) 23–31, https://doi.org/10.1515/aot-2017-0086.
[21] F. Rainer, W.H. Lowdermilk, D. Milam, C.K. Carniglia, T.T. Hart, T.L. Lichtenstein, Materials for optical coatings in the ultraviolet, Appl. Optic. 24 (1985) 496–500, https://doi.org/10.1364/ao.24.000496.
[22] J. DiJon, E. Quesnel, B. Rolland, P. Garrec, C. Pelle, J. Hue, High-damage-threshold fluoride UV mirrors made by ion-beam sputtering, Proc. SPIE 3244 (1998) 406–416, https://doi.org/10.1117/12.306989.
[23] K. Ferencz, Recent developments of laser optical coatings in Hungary, Opt. Eng. 32 (1993) 2525–2539, https://doi.org/10.1117/12.145356.
[24] C.J. Stolz, E. Feigenbaum, Impact of high refractive coating material on the nodular-induced electric field enhancement for near infrared multilayer mirrors, Appl. Optic. 59 (2020), https://doi.org/10.1364/ao.59.000a20. A20–A25.
[25] T. Willemsen, M. Jupé, M. Gyamfi, S. Schlichting, D. Ristau, Enhancement of the damage resistance of ultra-fast optics by novel design approaches, Optic Express 25 (2017) 31948–31959, https://doi.org/10.1364/oe.25.031948.
[26] C.J. Stolz, M. Caputo, A.J. Griffin, M.D. Thomas, BDS thin film UV antireflection laser damage competition, Proc. SPIE 7842 (2010) 6, https://doi.org/10.1117/12.867742.
[27] C. McDonagh, F. Sheridan, T. Butler, B.D. MacCraith, Characterisation of sol-gel-derived silica films, J. Non-Cryst. Solids 194 (1996) 72–77, https://doi.org/10.1016/0022-3093(95)00488-2.
[28] M.M. Collinson, H. Wang, R. Makote, A. Khramov, The effects of drying time and relative humidity on the stability of sol-gel derived silicate films in solution, J. Electroanal. Chem. 519 (2002) 65–71, https://doi.org/10.1016/S0022-0728(01)00723-9.
[29] Q. Mo, T. Shi, W. Cai, S. Zhao, D. Yan, J. Du, Z. Zang, Room temperature synthesis of stable silica-coated $CsPbBr_3$ quantum dots for amplified spontaneous emission, Photon. Res. 8 (2020) 1605–1612.
[30] H. Guan, S. Zhao, H. Wang, D. Yan, M. Wang, Z. Zang, Room temperature synthesis of stable single silica-coated $CsPbBr_3$ quantum dots combining tunable red emission of Ag–In–Zn–S for High-CRI white light-emitting diodes, Nanomater. Energy 67 (2020), 104279.
[31] M. Zhu, N. Xu, B. Roshanzadeh, S.T.P. Boyd, W. Rudolph, Y. Chai, J. Shao, Nanolaminate-based design for UV laser mirror coatings, Light Sci. Appl. 9 (2020) 1–6, https://doi.org/10.1038/s41377-020-0257-4.
[32] T. Tolenis, L. Grinevičiute, L. Smalakys, M. Ščiuka, R. Drazdys, L. Mažule, R. Buzelis, A. Melninkaitis, Next generation highly resistant mirrors featuring all-silica layers, Sci. Rep. 7 (2017) 1–9, https://doi.org/10.1038/s41598-017-11275-0.
[33] B.B. Burton, S.W. Rang, S.W. Rhee, S.M. George, SiO_2 atomic layer deposition using tris(dimethylamino)silane and hydrogen peroxide studied by in situ transmission FTIR spectroscopy, J. Phys. Chem. C 113 (2009) 8249–8257, https://doi.org/10.1021/jp806638e.
[34] M. Putkonen, M. Bosund, O.M.E. Ylivaara, R.L. Puurunen, L. Kilpi, H. Ronkainen, S. Sintonen, S. Ali, H. Lipsanen, X. Liu, E. Haimi, S.P. Hannula, T. Sajavaara, I. Buchanan, E. Karwacki, M. Vähä-Nissi, Thermal and plasma enhanced atomic layer deposition of SiO_2 using commercial silicon precursors, Thin Solid Films 558 (2014) 93–98, https://doi.org/10.1016/j.tsf.2014.02.087.
[35] Y. Wei, Q. Xu, Z. Wang, Z. Liu, F. Pan, Q. Zhang, J. Wang, Growth properties and optical properties for HfO_2 thin films deposited by atomic layer deposition, J. Alloys Compd. 735 (2018) 1422–1426, https://doi.org/10.1016/j.jallcom.2017.11.222.
[36] Y. Chai, M. Zhu, K. Yi, W. Zhang, H. Wang, Z. Fang, Z. Bai, Y. Cui, J. Shao, Experimental demonstration of laser damage caused by interface coupling effects of substrate surface and coating layers, Opt. Lett. 40 (2015) 3731–3734, https://doi.org/10.1364/ol.40.003731.
[37] L.H. Kim, K. Kim, S. Park, Y.J. Jeong, H. Kim, D.S. Chung, S.H. Kim, C.E. Park, Al_2O_3/TiO_2 nanolaminate thin film encapsulation for organic thin film transistors via plasma-enhanced atomic layer deposition, ACS Appl. Mater. Interfaces 6 (2014) 6731–6738, https://doi.org/10.1021/am500458d.
[38] S. Shestaeva, A. Bingel, P. Munzert, L. Ghazaryan, C. Patzig, A. Tünnermann, A. Szeghalmi, Mechanical, structural, and optical properties of PEALD metallic oxides for optical applications, Appl. Optic. 56 (2017), https://doi.org/10.1364/ao.56.000c47. C47–C59.
[39] T. Faraz, H.C.M. Knoops, M.A. Verheijen, C.A.A. Van Helvoirt, S. Karwal, A. Sharma, V. Beladiya, A. Szeghalmi, D.M. Hausmann, J. Henri, M. Creatore, W.M.M. Kessels, Tuning material properties of oxides and nitrides by substrate biasing during plasma-enhanced atomic layer deposition on planar and 3D substrate topographies, ACS Appl. Mater. Interfaces 10 (2018) 13158–13180, https://doi.org/10.1021/acsami.8b00183.
[40] C. Yin, M. Zhu, C. Song, T. Zeng, N. Xu, Y. Wang, Y. Zhao, K. Yi, J. Shao, Influence of deposition temperature and precursor pulse time on properties of SiO_2, HfO_2 monolayers deposited by PEALD, Proc. SPIE 11064 (2019) 17, https://doi.org/10.1117/12.2539917.
[41] H. Hou, K. Yi, S. Shang, J. Shao, Z. Fan, Measurements of light scattering from glass substrates by total integrated scattering, Appl. Optic. 44 (2005) 6163–6166, https://doi.org/10.1364/AO.44.006163.
[42] S. Fan, H. He, J. Shao, Z. Fan, D. Zhang, Absorption measurement for coatings using surface thermal lensing technique, Proc. SPIE 5774 (2004) 531–534, https://doi.org/10.1117/12.607475.
[43] B.V. Crist, Argon implanted into graphite, by XPS, Surf. Sci. Spectra 1 (1992) 376–380, https://doi.org/10.1116/1.1247636.
[44] J.C. Hackley, T. Gougousi, Properties of atomic layer deposited HfO_2 thin films, Thin Solid Films 517 (2009) 6576–6583, https://doi.org/10.1016/j.tsf.2009.04.033.
[45] X.L. Wei, M. Fahlman, A.J. Epstein, XPS study of highly sulfonated polyaniline, Macromolecules 32 (1999) 3114–3117, https://doi.org/10.1021/ma981386p.
[46] B.M. Reddy, B. Chowdhury, P.G. Smirniotis, XPS study of the dispersion of MoO_3 on TiO_2-ZrO_2, TiO_2-SiO_2, TiO_2-Al_2O_3, SiO_2-ZrO_2, and SiO_2-TiO_2-ZrO_2 mixed oxides, Appl. Catal. Gen. 211 (2001) 19–30, https://doi.org/10.1016/S0926-860X(00)00834-6.
[47] H. Dong, K. Chen, P. Zhang, W. Li, J. Xu, Z. Ma, Z. Sun, Z. Liu, The role of N_x-Si-O_y bonding configuration in acquiring strong blue to red photoluminescence from amorphous SiN_xO_y film, Can. J. Phys. 92 (2014) 602–605, https://doi.org/10.1139/cjp-2013-0609.
[48] T. Harada, H. Murotani, S. Matumoto, H. Honda, Influence of substrate surface roughness on light scattering of TiO_2 optical thin films, Chin. Optic Lett. 11 (2013) 10303.
[49] J. Fan, H. Liu, Q. Kuang, B. Gao, F. Ma, Y. Hao, Physical properties and electrical characteristics of H_2O-based and O_3-based HfO_2 films deposited by ALD, Microelectron. Reliab. 52 (2012) 1043–1049, https://doi.org/10.1016/j.microrel.2012.01.010.
[50] D. Barreca, A. Milanov, R.A. Fischer, A. Devi, E. Tondello, Hafnium oxide thin film grown by ALD: an XPS study, Surf. Sci. Spectra 14 (2007) 34–40, https://doi.org/10.1116/11.20080401.
[51] C.S. Kang, H.J. Cho, K. Onishi, R. Nieh, R. Choi, S. Gopalan, S. Krishnan, J.H. Han, J.C. Lee, Bonding states and electrical properties of ultrathin HfO_xN_y gate dielectrics, Appl. Phys. Lett. 81 (2002) 2593–2595, https://doi.org/10.1063/1.1510155.
[52] F. Hirose, Y. Kinoshita, K. Kanomata, K. Momiyama, S. Kubota, K. Hirahara, Y. Kimura, M. Niwano, IR study of fundamental chemical reactions in atomic layer deposition of HfO_2 with tetrakis(ethylmethylamino)hafnium (TEMAH), ozone, and water vapor, Appl. Surf. Sci. 258 (2012) 7726–7731, https://doi.org/10.1016/j.apsusc.2012.04.130.
[53] R.D. Clark, A. Hochberg, M. Jahl, K. Cuthill, T. Kok, A chemists view of precursors and processes for the production of Hf-based high K dielectrics, ECS Trans 1 (2019) 201–209, https://doi.org/10.1149/1.2209269.
[54] S. Papernov, M.D. Brunsman, J.B. Oliver, B.N. Hoffman, A.A. Kozlov, S.G. Demos, A. Shvydky, F.H.M. Cavalcante, L. Yang, C.S. Menoni, B. Roshanzadeh, S.T.P. Boyd, L.A. Emmert, W. Rudolph, Optical properties of oxygen vacancies in HfO_2 thin films studied by absorption and luminescence spectroscopy, Optic Express 26 (2018) 17608–17623, https://doi.org/10.1364/oe.26.017608.
[55] R.L. Puurunen, Surface chemistry of atomic layer deposition: a case study for the trimethylaluminum/water process, J. Appl. Phys. 97 (2005), 121301, https://doi.org/10.1063/1.1940727.
[56] N. Xu, M. Zhu, Y. Chai, B. Roshanzadeh, S.T.P. Boyd, W. Rudolph, Y. Zhao, R. Chen, J. Shao, Laser resistance dependence of interface for high-reflective coatings studied by capacitance-voltage and absorption measurement, Opt. Lett. 43 (2018) 4538–4541, https://doi.org/10.1364/ol.43.004538.
[57] N. Xu, M. Zhu, Y. Chai, B. Roshanzadeh, S.T.P. Boyd, W. Rudolph, Y. Zhao, R. Chen, J. Shao, Laser resistance dependence of interface for high-reflective coatings studied by capacitance-voltage and absorption measurement, Opt. Lett. 43 (2018) 4538–4541, https://doi.org/10.1364/ol.43.004538.
[58] J. Dijon, G. Ravel, B. Andre, Thermomechanical model of mirror laser damage at 1.06 um: II. Flat bottom pits formation, Proc. SPIE 3578 (1999) 398–407.
[59] H. Wang, H. Qi, W. Zhang, J. Sun, Y. Chai, F. Tu, J. Zhao, Z. Yu, B. Wang, M. Zhu, Suppression of nano-absorbing precursors and damage mechanism in optical coatings for 3ω mirrors, Opt. Lett. 41 (2016) 1209–1212.
[60] G. Abromavičius, S. Kičas, R. Buzelis, High temperature annealing effects on spectral, microstructural and laser damage resistance properties of sputtered HfO_2 and HfO_2-SiO_2 mixture-based UV mirrors, Opt. Mater. 95 (2019), 109245, https://doi.org/10.1016/j.optmat.2019.109245.
[61] T.J. Park, Y. Byun, R.M. Wallace, J. Kim, Reduced impurities and improved electrical properties of atomic-layer-deposited HfO_2 film grown at a low temperature (100 °C) by Al_2O_3 incorporation, Appl. Surf. Sci. 371 (2016) 360–364, https://doi.org/10.1016/j.apsusc.2016.02.243.